CONSTRAINED GRAPH MECHANICS NETWORKS

Anonymous authors
Paper under double-blind review

ABSTRACT

Learning to reason about relations and dynamics over multiple interacting objects is a prevailing yet challenging topic in machine learning. The challenges mainly stem from that interacting systems are of combinatorial complexity, the model we learn should obey Euclidean equivariance, and certain geometrical constraints commonly exist. Current methods, particularly the ones based on equivariant Graph Neural Networks (GNNs), have targeted on the first two challenges but remain immature for constrained systems. In this paper, we propose Graph Mechanics Network (GMN) which is combinatorially efficient, equivariant and constraint-aware. The core of GMN is that it represents, by generalized coordinates, the forward kinematics information (positions and velocities) of a structural object. In this manner, the geometrical constraints are implicitly and naturally encoded in the forward kinematics. Moreover, to allow equivariant message passing in GMN, we have developed a general form of orthogonality-equivariant functions, given that the dynamics of constrained systems are more complicated than the unconstrained counterparts. Theoretically, the proposed equivariant formulation is proved to be universally expressive under certain conditions. Simulated experiments on particles, sticks, hinges, and the combinations of them support the advantages of GMN compared to the state-of-the-art GNNs in terms of prediction accuracy, constraint satisfaction and data efficiency.

1 INTRODUCTION

Representing and reasoning about the relations and dynamics of a group of interacting objects is among the core aspects of human intelligence (Tenenbaum et al., 2011). As a motivating example, we consider the N-body system (Kipf et al., 2018) where the movement of a single charged particle is attracted or repelled by other charged particles. Physicists have revealed that this process can be modeled by Newton's laws along with the Coulombian force. One may wonder, however, if we can teach a machine to rediscover the underlying physics by solely observing the particles' states, just like what physicists used to do, first recording data and then inducting formulas. This thinking has actually inspired the study of learning to model interacting systems, which now is a prevailing topic in machine learning (Battaglia et al., 2016; Thomas et al., 2018; Köhler et al., 2019; Sanchez-Gonzalez et al., 2019; Fuchs et al., 2020; Martinkus et al., 2021; Satorras et al., 2021).

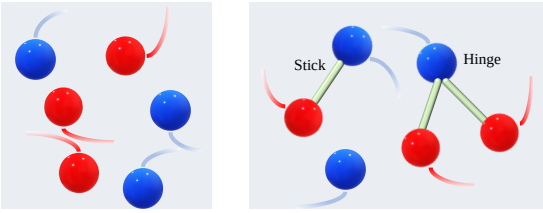

(a) N-body System (b) Constrained N-body System

Figure 1: The N-body system (Kipf et al., 2018) vs. the constrained N-body system, where the red/blue balls denote positive/negative charges.

Learning to model interacting systems is challenging. First, the systems are combinatorially complex, on account of that objects can be composed in combinatorially many possible arrangements (Battaglia et al., 2016). This challenge, to some extent, can be addressed by making use of Graph Neural Networks (GNNs) (Wu et al., 2020). By regarding objects as nodes and interactions as edges, GNNs extract information via message passing, which is able to characterize arbitrarily ordered objects and combinatorial relations. The second challenge is related to an important symmetry

in physics: the model we use should be equivariant to any Euclidean transformation (translation or rotation) of the input states. This complies with the fact that physics rules keep unchanged regardless of the reference coordinate system. Several works (Fuchs et al., 2020; Satorras et al., 2021) have investigated equivariance upon GNNs and exhibited remarkable benefits on the N-body system.

Another challenge, though less explored, is that the systems could be geometrically constrained. Geometric constraints arise in common practical systems, for example, in robotics where the joints of mechanical arms should be linked one by one, or in biochemistry where the atoms of molecules are connected by chemical bonds. When modeling these constrained systems, it is crucial to enforce the model to output legal predictions. For instance, the lengths/angles of chemical bonds in a molecular closely determine its chemical property which will be changed dramatically if the structural constraints are broken. As mentioned above, equivariant GNNs (Fuchs et al., 2020; Satorras et al., 2021) have achieved desired performance on the N-body system—this system, nevertheless, lacks of constraint. Considering constraints, by no means, is not easy, as the dynamics of all elements within a constrained system evolve in a joint and complex manner. Unfortunately, to the best of our knowledge, there is no research (particularly among equivariant GNN methods) that learns to model the dynamical systems of multiple interacting objects under geometrical constraints.

In this paper, we propose Graph Mechanics Network (GMN) that can tackle the above three challenges simultaneously: **I.** To cope with the combinatorial complexity, GMN takes advantage of graph models to encode the states of and interactions between objects, analogous to previous approaches. **II.** For the constraint satisfaction, GMN resorts to generalized coordinates, a well known notion in conventional mechanics to model the dynamics of structural objects. Here, a structural object (such as the stick and hinge in Fig. 1) is defined as a set of multiple rigidly connected particles. In GMN, the constraints are implicitly encoded in the forward kinematics that describes the Cartesian states as the function of generalized coordinates. This strategy can inherently maintain the constraints and requires no external regulation. **III.** GMN is equivariant. In GMN, we need to compute the interaction forces in the Cartesian space (see Eq. 5), and infer the accelerations of the generalized coordinates based on the inverse dynamics (see Eq. 6), both of which are learned by a general form of equivariant functions (see Eq. 11). Notably, the proposed equivariant formulation is more efficient to compute compared to the previous versions based on spherical harmonics (Thomas et al., 2018; Fuchs et al., 2020), or more general than the one developed by EGNN (Satorras et al., 2021). More importantly, we have theoretically discussed when and how our formulation can universally approximate any equivariant function.

To evaluate the advantages of GMN, we have constructed a simulated dataset composed of three types of objects: particles, sticks and hinges, which is a complex case of the N-body system (Kipf et al., 2018) and can be used as building blocks for common systems. Under various scenarios in terms of different ratios of object types and different numbers of training data, we empirically verify the superiority of GMN compared to state-of-the-art models in prediction accuracy, constraint satisfaction and data efficiency.

2 Related Work

Learning to simulate complex physical systems has been shown to greatly benefit from using GNNs. Interaction Network (IN) proposed by Battaglia et al. (2016) is the first attempt for this purpose, and it can be deemed as a special kind of GNNs to learn how the system interacts and how the states of particles evolve. Later researches have extended IN in different aspects: HRN (Mrowca et al., 2018) utilizes hierarchical graph convolution for tackling objects of various geometrical shapes and materials, NRI (Kipf et al., 2018) further explicitly infers the interactions with the help of a variational auto-encoder, and Hamiltonian graph networks (Sanchez-Gonzalez et al., 2019) equip GNNs with ordinary differential equations and Hamiltonian mechanics for energy conservation. However, all above approaches have ignored the symmetry in physics and the GNN models they use are not Euclidean equivariant. On the other hand, it is nontrivial to enforce equivariance. Tensor-Field networks (Thomas et al., 2018) uses filters built from spherical harmonics to allow 3D rotation equivariance, and this idea has been developed by SE(3) Transformer (Fuchs et al., 2020) that further takes the attention mechanism into account. Anther class of works (Finzi et al., 2020a; Hutchinson et al., 2021) resorts to the Lie convolution for the equivariance on any Lie group, based on lifting and sampling. Recently, EGNN (Satorras et al., 2021) has proposed a simple yet effective form of

equivariant message passing on graphs, which does not require computationally expensive higher-order representations while still achieving better performance on the N-body system.

As interpreted before, ensuring geometrical constraints is crucial for many practical systems, which, nevertheless, is seldom investigated in aforementioned works. Although several attempts (Yang et al., 2020; Finzi et al., 2020b) have been proposed for learning to enforce constraints, they explicitly augment the training loss with soft Lagrangian regulation and thus are completely data-driven and have no guarantee of generalization for limited training data. Further, these methods only target on the physical process of a single object, other than the complex systems with multiple interacting objects that are the focus of this paper. Besides, they never study equivariant models. By contrast, our GMN is equivariant and naturally meets the constraints for interacting systems.

3 Graph Mechanics Neural Network

3.1 Notations and Preliminaries

We begin with introducing the N-body system (Kipf et al., 2018), as illustrated in Fig. 1 (a). This system consists of N interacting particles $\{P_i\}_{i=1}^N$ of the same mass, and the kinematics states of each particle are defined as $\boldsymbol{S}_i = (\boldsymbol{x}_i, \boldsymbol{v}_i)$, where $\boldsymbol{x}_i, \boldsymbol{v}_i \in \mathbb{R}^3$ are the position and velocity vectors, respectively. There could be certain non-vector information of each particle (such as charge), which is represented by a c-channel feature $h_i \in \mathbb{R}^c$ [1]. Suppose the system we study is conservative and the dynamics is driven by the interaction force $\boldsymbol{f}_{ij} \in \mathbb{R}^3$ between any pair of particles i and j. According to Newton's second law, the acceleration of particle i, $\boldsymbol{a}_i \in \mathbb{R}^3$ is proportion to the its aggregated force from other particles $\sum_{j \neq i} \boldsymbol{f}_{ij}$. All symbols will be specified with a superscript t for temporal denotations, *e.g.*, $\boldsymbol{x}_i^t$ indicating the position of particle i at time t. In this paper, we are mainly concerned with the prediction task: we need to seek out a function $\phi(\{(\boldsymbol{S}_i^0, h_i^0)\}_{i=1}^N)$ given the initial states $\{\boldsymbol{S}_i^0\}_{i=1}^N$ and features $\{h_i^0\}_{i=1}^N$ to forecast the future states $\{\boldsymbol{S}_i^T\}_{i=1}^N$ at time T.

As presented in Introduction, two kinds of inductive biases have been explored previously. The first one is to apply the graph structure to capture the distribution of particle states and their interactions (Battaglia et al., 2016; Kipf et al., 2018), where, particularly, the particle states $\boldsymbol{S}_i^0$ (along with h_i^0) are as node features and the interaction forces $\boldsymbol{f}_{ij}^0$ as edge messages. In this way, the transition function ϕ boils down to a GNN model. The second inductive bias is that ϕ should be equivariant to any translation/rotation of the input states. By saying equivariance, we mathematically imply that

$$\phi(\{(g \cdot \boldsymbol{S}_i^0, h_i^0)\}_{i=1}^N) = g \cdot \phi(\{(\boldsymbol{S}_i^0, h_i^0)\}_{i=1}^N), \forall g \in \mathrm{SE}(3), \forall \boldsymbol{S}_i^0, \forall h_i^0. \tag{1}$$

Here, SE(3) defines the 3D Euclidean group (Fuchs et al., 2020) that consists of translation and rotation transformations; $g \cdot \boldsymbol{S}_i^0$ denotes to perform transformation g on the states $\boldsymbol{S}_i^0$, and it is instantiated as $\boldsymbol{R}(\boldsymbol{x}_i^0 + \boldsymbol{b})$ for the position and $\boldsymbol{R}\boldsymbol{v}_i^0$ for the velocity, where $\boldsymbol{R} \in \mathbb{R}^{3\times 3}$ is the rotation matrix and $\boldsymbol{b} \in \mathbb{R}^3$ is the translation vector.

Several works (Thomas et al., 2018; Köhler et al., 2019; Fuchs et al., 2020; Satorras et al., 2021) have investigated both inductive biases, among which EGNN (Satorras et al., 2021) has achieved promising performance on N-body. The typical process in EGNN iterates the following steps:

$$\boldsymbol{a}_i^l, h_i^l = \sum_j \varphi_{\text{egnn}}(\boldsymbol{x}_{ji}^{l-1}, h_i^{l-1}, h_j^{l-1}, e_{ji}), \tag{2}$$

$$\boldsymbol{v}_i^l = \psi(h_i^{l-1})\boldsymbol{v}_i^{l-1} + \boldsymbol{a}_i^l, \tag{3}$$

$$\boldsymbol{x}_i^l = \boldsymbol{x}_i^{l-1} + \boldsymbol{v}_i^l, \tag{4}$$

where, the superscript l denotes the l-th layer; the acceleration $\boldsymbol{a}_i^l$ returned by the message aggregation of φ_{egnn} in Eq. 2 is adopted for the update of the velocity $\boldsymbol{v}_i^l$ in Eq. 3 (multiplied by a scalar $\psi(h_i^{l-1}) \in \mathbb{R}$), followed by the renovation of the position $\boldsymbol{x}_i^l$ in Eq. 4. The formulation of φ_{egnn} is physically reasonable, since the interaction (actually the Coulombian force) between particles i and j truly depends on their relative position $\boldsymbol{x}_{ji}^{l-1} = \boldsymbol{x}_i^{l-1} - \boldsymbol{x}_j^{l-1}$, node features h_i^{l-1} and h_j^{l-1}, and

[1] Although h_i could be of multiple dimensions, we still call it as a non-vector value since the dimension of h_i is distinct from that of the kinematics vector, for example $\boldsymbol{x}_i$, the latter of which has intrinsic geometry and should obey translation/rotation equivariance. This is also why we do not denote h_i in bold.

edge feature e_{ji}. To enable equivariance message passing, EGNN has developed a specific form of φ_{egnn} to let $\boldsymbol{a}_i^l$ be equivariant and h_i^l be invariant in terms of the input $\boldsymbol{x}_{ji}^{l-1}$, as presented in Eq. 10.

3.2 Our General Architecture

Despite the desired performance on N-body, existing methods are incapable of maintaining the geometric constraint. In this section, we design a general architecture that intrinsically meets the requirement of geometry constraints by making use of the generalized coordinates. The main idea is that the constraints are implicitly and exactly encoded in the forward kinematics that represents the Cartesian states of the system as the function of generalized coordinates.

We define $\mathcal{O}_k = \{P_i\}_{i=1}^{n_k}$ a structural object composed of n_k rigidly connected particles. Fig. 1 (b) illustrates two examples of the structural object, the stick with 2 connected particles and the hinge with 3 particles. To preserve the distance, the dynamics of the two particles on a stick should be updated in a joint way, rather than fulfilling the independent process in EGNN (Eq. 3 and 4). Besides, the force on each particle within $\mathcal{O}_k$ will indirectly influence the dynamics of others through the physical connections. This requires us to analyze the dynamics of the particles in $\mathcal{O}_k$ as a whole, which is implemented by generalized coordinates. There could be multiple generalized coordinates for each $\mathcal{O}_k$, some located in the Cartesian space but some in the angle space. For instance, the states of a stick can be decoupled by two independent sets of generalized coordinates: the state of particle 1 as the Cartesian coordinates and the relative rotation angles of particle 2 to 1 as the angle coordinates. For conciseness, the introductions in this section only focus on the Cartesian part which essentially determines the local coordinates in $\mathcal{O}_k$, with providing full details for the examples in § 3.4. We denote the position, velocity and acceleration of the generalized Cartesian coordinates as $\boldsymbol{q}_k$, $\dot{\boldsymbol{q}}_k$ and $\ddot{\boldsymbol{q}}_k$, respectively.

We now detail how to update the states of $\mathcal{O}_k$. In Fig. 2, we first compute the interaction force between each particle and others, and aggregate information of all particles within each structural object to inference the acceleration of the generalized coordinates (which is termed as the generalized acceleration henceforth) by inverse dynamics. Then, the dynamical updates are carried out in the space of the generalized coordinates. Finally, the updated generalized coordinates will be projected back to the particles' states via the forward kinematics. In form,

$$\boldsymbol{f}_i^l, h_i^l = \sum_j \varphi_1(\boldsymbol{x}_{ji}^{l-1}, h_i^{l-1}, h_j^{l-1}, e_{ji}), \quad (5)$$

$$\ddot{\boldsymbol{q}}_k^l = \sum_{i \in \mathcal{O}_k} \varphi_2(\boldsymbol{f}_i^l, \boldsymbol{x}_{ki}^{l-1}, \boldsymbol{v}_{ki}^{l-1}), \quad (6)$$

$$\dot{\boldsymbol{q}}_k^l = \psi(\sum_{i \in \mathcal{O}_k} h_i^{l-1})\dot{\boldsymbol{q}}_k^{l-1} + \ddot{\boldsymbol{q}}_k^l, \quad (7)$$

$$\boldsymbol{q}_k^l = \boldsymbol{q}_k^{l-1} + \dot{\boldsymbol{q}}_k^l, \quad (8)$$

$$\boldsymbol{x}_i^l, \boldsymbol{v}_i^l = \text{FK}(\boldsymbol{q}_k^l, \dot{\boldsymbol{q}}_k^l), \forall i \in \mathcal{O}_k, \quad (9)$$

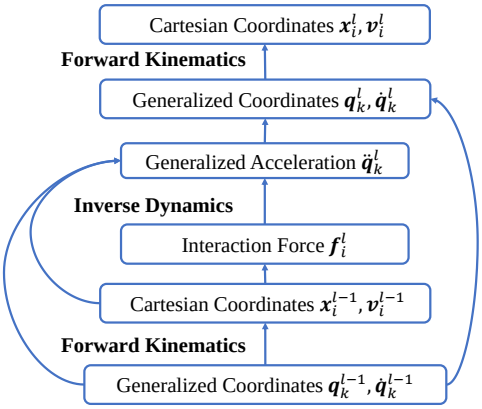

Figure 2: The flowchart of our GMN.

where, the elements of the system can be described in two views, $\{\mathcal{O}_k\}_{k=1}^K$ as the object-level view and $\{P_i\}_{i=1}^N$ as the particle-level view; for distinction, we index the structural object with the subscript k and particles with i or j. We explain each equation separately.

Interaction force (Eq. 5). The interaction force $\boldsymbol{f}_i^l$ is computed analogous to Eq. 2. EGNN straightly regards the interaction force to be the acceleration of each particle in Eq. 2. But here, given the constraints between particles, we record the force as an intermediate variable that will contribute to the inference of the generalized acceleration in the next step.

Inverse dynamics (Eq. 6). This step is the core of our methodology. The generalized acceleration $\ddot{\boldsymbol{q}}_k^l$ is dependent to the forces $\boldsymbol{f}_i^l$ on all particles within $\mathcal{O}_k$, and their relative positions $\boldsymbol{x}_{ki}^{l-1} = \boldsymbol{x}_i^{l-1} - \boldsymbol{q}_k^{l-1}$ and relative velocities $\boldsymbol{v}_{ki}^{l-1} = \boldsymbol{v}_i^{l-1} - \dot{\boldsymbol{q}}_k^{l-1}$ with regard to the generalized coordinates. The formulation of Eq. 6 is physics-inspired. In Appendix (Eq. 27), we have analytically derived the dynamics of hinges, where the acceleration of the hinge is indeed related to the

forces, relative positions and relative velocities of all particles in each hinge. This is reasonable in mechanics, since the cross product $\boldsymbol{x}_{ki}^{l-1} \times \boldsymbol{f}_i^l$ yields the torque, and the relative velocity $\boldsymbol{v}_{ki}^{l-1}$ is related to the centrifugal force of particle i around $\boldsymbol{q}_k$, both of which influence the acceleration $\ddot{\boldsymbol{q}}_k$. Different from the analytical form which is always complex and hard to compute in practice, we will employ a learnable and equivariant function with universal expressivity. The details are in § 3.3.

Generalized update (Eq. 7-8). The updates of the generalized coordinates are akin to Eq. 3 and 4 in EGNN, as the dimensions of the generalized coordinates have been made independent. Notice that in Eq. 7 the scalar factor for $\dot{\boldsymbol{q}}_k^{l-1}$ takes as input the summation of all hidden features, which is a generalized form of Eq. 3 for multiple particles in $\mathcal{O}_k$.

Forward kinematics (Eq. 9). Once the generalized coordinates have been refreshed, we can derive the states of all particles in $\mathcal{O}_k$ by proceeding the forward kinematics. Different system of $\mathcal{O}_k$ could have different type of the forward kinematics. Here we denote it as the function $\text{FK}(\cdot)$ in general, while providing the specifications in § 3.4.

Although our method is initially targeted on structural objects, it is still applicable for free particles, if we set the generalized coordinates as the states of each particle and utilize the trivial forward kinematics (the identity mapping) in Eq. 9. Alg. 1 has summarized the updates for all structural objects layer by layer.

3.3 Equivariant Message Passing

As shown in Eq. 1, the SE(3) equivariance on the estimation function ϕ is necessary for ensuring the physical symmetry. When considering this property in our case, we demand the interaction force (Eq. 5) and generalized acceleration (Eq. 6) to be equivariant with respect to rotations, while other equations are already equivariant[2]. EGNN (Satorras et al., 2021) has developed a particular rotation-equivariant form for the acceleration output in Eq. 2:

$$\varphi_{\text{egnn}}(\boldsymbol{x}, h) \coloneqq \boldsymbol{x}\rho_w(\|\boldsymbol{x}\|_2^2, h), \tag{10}$$

where $\rho_w(\cdot)$ is an arbitrary Multi-Layer Perceptron (MLP) with parameter w, and we have abbreviated other non-vector terms in Eq. 2 as h. This formulation does satisfy the rotation equivariance, but it is unknown if it can be generalized to the function (such as Eq. 6) with multiple input vectors, and more importantly, its representation completeness is never explored rigorously. In this section, we propose a general form of orthogonality-equivariant functions with necessary theoretical guarantees.

Without loss of generality, the target function we would like to enforce equivariance is denoted as $\varphi(\boldsymbol{Z}, h) : \mathbb{R}^{d\times m} \times \mathbb{R}^c \to \mathbb{R}^{d\times m'}$. We define the below formulation,

$$\varphi(\boldsymbol{Z}, h) \coloneqq \boldsymbol{Z}\rho_w(\boldsymbol{Z}^\top \boldsymbol{Z}, h). \tag{11}$$

It is easy to justify the function $\varphi(\boldsymbol{Z}, h)$ in Eq. 11 is equivariant to any orthogonal matrix *i.e.*, $\varphi(\boldsymbol{O}\boldsymbol{Z}, h) = \boldsymbol{O}\varphi(\boldsymbol{Z}, h), \forall \boldsymbol{O} \in \mathbb{R}^{d\times d}, \boldsymbol{O}^\top\boldsymbol{O} = \boldsymbol{I}$. Apparently, Eq. 11 reduces to Eq. 10 by setting the number of vectors in $\boldsymbol{Z}$ as 1, namely, $m = m' = 1$. We immediately have the following theory.

Theorem 1. *If $m \geq d$ and the row rank of $\boldsymbol{Z}$ is full,* i.e. *rank$(\boldsymbol{Z}) = d$, then for any continuous orthogonality-equivariant function $\hat{\varphi}(\boldsymbol{Z}, h)$, there must exist an MLP ρ_w satisfying $\|\varphi(\boldsymbol{Z}, h) - \hat{\varphi}(\boldsymbol{Z}, h)\| < \epsilon$ for arbitrarily small error ϵ.*

The proof employs the universality of MLP (Cybenko, 1989; Hornik, 1991), with the entire details deferred in Appendix. Theorem 1 is nutritive, as it characterizes the rich expressivity of formulating the equivariant function via Eq. 11. The condition holds in general for the function like Eq. 6 whose input $\boldsymbol{Z} = (\boldsymbol{f}_i, \boldsymbol{x}_{ki}, \boldsymbol{v}_{ki}) \in \mathbb{R}^{3\times 3}$ is of full rank when the force, position and velocity expand the whole space. Indeed, this condition holds with probability 1, stated by the following corollary.

Corollary 1. *Assume $m \geq d$, and also the entries of $\boldsymbol{Z}$ are drawn independently from a distribution that is absolutely continuous with respect to the Lebesgue measure in $\mathbb{R}$. Then, almost surely, the conclusion of Theorem 1 holds.*

When the condition $m \geq d$ is invalid, the universal approximation still maintains if restricted in the linear subspace expanded by the columns of $\boldsymbol{Z}$.

[2]The translation equivariance holds naturally as we use relative positions in Eq. 5, making the force, acceleration, velocity to be invariant with respect to translation. After the addition with the previous position in Eq. 8, the updated position $\boldsymbol{q}_k^l$ is translation equivariant.

Corollary 2. *For any continuous orthogonality-equivariant function $\hat{\varphi}(\boldsymbol{Z}, h)$ whose output is located in the linear subspace expanded by the columns of $\boldsymbol{Z}$, the conclusion of Theorem 1 holds universally.*

Corollary 2 tells that the message passing φ_{egnn} in Eq. 10 is not universally expressive since $m < d$, and can only fit the vectors parallel to $\boldsymbol{x}$ (*i.e.* the relative position). Yet, φ_{egnn} is physically complete for the Coulombian force that is oriented by the relative position between two particles.

In our experiments, we find that more stable performance is delivered by further adding the normalization term specifically when $m > 1$:

$$\varphi(\boldsymbol{Z}, h) := \boldsymbol{Z}\rho_w(\frac{\boldsymbol{Z}^\top \boldsymbol{Z}}{\|\boldsymbol{Z}^\top \boldsymbol{Z}\|_F}, h), \tag{12}$$

where $\|\cdot\|_F$ computes the Frobenius norm. Notice that adding normalization does not change the conclusions in Theorem 1 and its two corollaries, since the norm is also a function of $\boldsymbol{Z}^\top \boldsymbol{Z}$ that can be approximated by MLP. We implement φ_1 in Eq. 5 and φ_2 in Eq. 6 by using the general formulation Eq. 12, where $\boldsymbol{Z} = \boldsymbol{x}_{ji}^{l-1}$ and $\boldsymbol{Z} = (\boldsymbol{f}_i^l, \boldsymbol{x}_{ki}^{l-1}, \boldsymbol{v}_{ki}^{l-1})$, respectively. Note that for the update of hidden feature h_i^l in Eq. 5, we do not need equivariance but invariance, hence we set $h_i^l = \rho_w(\frac{\boldsymbol{Z}^\top \boldsymbol{Z}}{\|\boldsymbol{Z}^\top \boldsymbol{Z}\|_F}, h_i^{l-1})$ by just keeping the invariant part in Eq. 12.

3.4 Implementations by Considering Generalized Angles

In this section, we take the hinge and stick as two examples to show how to consider generalized angels. We assume the interaction forces only act on the particles.

Implementation of hinges. A hinge, as displayed in Fig.3 (a), consists of three particles 0, 1, 2, and two sticks 01 and 02. The freedom degrees of this system can be explained in this way: particle 0 moves freely, and particles 1 and 2 can only rotate round particle 0 owing to the length constraint by the two sticks. Hence, the generalized coordinates include the states of particle 0 denoted as $\boldsymbol{q}_0 \in \mathbb{R}^3$ and the rotation Euler angles of stick 01 as $\boldsymbol{\theta}_{01} \in \mathbb{R}^3$ and 02 as $\boldsymbol{\theta}_{02} \in \mathbb{R}^3$. As $\boldsymbol{q}_0$ are Cartesian, the dynamical update follows directly Eq. 5-8. With the forces $\{\boldsymbol{f}_i^l\}_{i=0}^3$ estimated in Eq. 5 and acceleration $\ddot{\boldsymbol{q}}_0^l$ by Eq. 6, the angle acceleration of $\boldsymbol{\theta}_{01}$ is calculated as $\ddot{\boldsymbol{\theta}}_{01}^l = \frac{\boldsymbol{x}_{01}^{l-1} \times (\boldsymbol{f}_1^l - \ddot{\boldsymbol{q}}_0^l)}{\|\boldsymbol{x}_{01}^{l-1}\|^2}$ according to rigid mechanics, where the numerator is the relative torque, the denominator is the moment of inertia under unit mass, and $\times$ means the cross product. Then the angle velocity is $\dot{\boldsymbol{\theta}}_{01}^l = \psi'(h_0^{l-1} + h_1^{l-1} + h_2^{l-1})\dot{\boldsymbol{\theta}}_{01}^{l-1} + \ddot{\boldsymbol{\theta}}_{01}^l$ similar to Eq. 7. We do not need to record $\boldsymbol{\theta}_{01}$, since the forward kinematics can be conducted without it. In detail, the forward kinematics in Eq. 9 is:

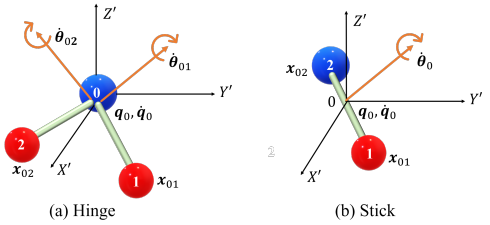

(a) Hinge (b) Stick

Figure 3: Generalized coordinates of hinges and sticks.

$$\boldsymbol{x}_1^l = \boldsymbol{q}_0^l + \text{rot}(\dot{\boldsymbol{\theta}}_{01}^l)\boldsymbol{x}_{01}^{l-1}, \tag{13}$$

$$\boldsymbol{v}_1^l = \dot{\boldsymbol{q}}_0^l + \dot{\boldsymbol{\theta}}_{01}^l \times \boldsymbol{x}_{01}^l, \tag{14}$$

where $\text{rot}(\dot{\boldsymbol{\theta}}_{01}^l)$ indicates the rotation matrix around the direction of $\dot{\boldsymbol{\theta}}_{01}^l$ by absolute angle $\|\dot{\boldsymbol{\theta}}_{01}^l\|$. The dynamic updates for particle 2 is similar. We put the whole details into Alg. 1 in Appendix.

Implementation of sticks. For a stick with particles 1 and 2 in Fig 3 (b), we choose the center as the generalized Cartesian coordinate $\boldsymbol{q}_0$, and the rotation of particle 1 $\boldsymbol{\theta}_{01}$ and particle 2 $\boldsymbol{\theta}_{02}$ ($\boldsymbol{\theta}_{01} = \boldsymbol{\theta}_{02}$) as the generalized angle coordinates. The dynamics propagation of $\boldsymbol{q}_0$ is given by Eq. 5-8. There are two choices to compute $\ddot{\boldsymbol{q}}_0^l$, one using the general form in Eq. 6 and the other one leveraging a simplified version as $\ddot{\boldsymbol{q}}_0^l = \sum_{i \in \mathcal{O}_k} \varphi(\boldsymbol{f}_i^l)$ by explicitly omitting the relative position and velocity. The physical motivation of introducing the simplified version is that the acceleration of a stick center is only affected by the forces according to the theorem of the motion of the center of mass. The angle accelerations are $\ddot{\boldsymbol{\theta}}_{01}^l = \frac{\boldsymbol{x}_{01}^{l-1} \times \boldsymbol{f}_1^l + \boldsymbol{x}_{02}^{l-1} \times \boldsymbol{f}_2^l}{\|\boldsymbol{x}_{01}^{l-1}\|^2 + \|\boldsymbol{x}_{02}^{l-1}\|^2}$, and the velocity becomes $\dot{\boldsymbol{\theta}}_{01}^l = \psi'(h_1^{l-1} + h_2^{l-1})\dot{\boldsymbol{\theta}}_{01}^{l-1} + \ddot{\boldsymbol{\theta}}_{01}^l$. Then the states of particles 1 and 2 are renewed as the same as Eq. 13-14.

Table 1: Prediction error ($\times 10^{-2}$) on various types of systems. The header of each column "p, s, h" denotes the scenario with p isolated particles, s sticks and h hinges. Note that the standard deviation of GMN over 3 runs is small (< 0.05), hence it is omitted in the table.

	|Train| = 500					|Train| = 1500				
	1,2,0	2,0,1	3,2,1	0,10,0	5,3,3	1,2,0	2,0,1	3,2,1	0,10,0	5,3,3
Linear	8.23	7.55	9.76	11.36	11.62	8.22	7.55	9.76	11.36	11.62
GNN	5.33	5.01	7.58	9.83	9.77	3.61	3.23	4.73	7.97	7.91
TFN	11.54	9.87	11.66	13.43	12.23	5.86	4.97	8.51	11.21	10.75
SE3-Tr.	5.54	5.14	8.95	11.42	11.59	5.02	4.68	8.39	10.82	10.85
RF	3.50	3.07	5.25	7.59	7.73	2.97	2.19	3.80	5.71	5.66
EGNN	2.81	2.27	4.67	4.75	4.59	2.59	1.86	2.54	2.79	3.25
EGNNReg	2.94	2.66	7.01	5.03	6.31	2.74	1.58	2.62	3.03	3.07
GMN	**1.84**	**2.02**	**2.48**	**2.92**	**4.08**	**1.68**	**1.47**	**2.10**	**2.32**	**2.86**

4 EXPERIMENTS

Datasets. Our datasets are generated via simulation. We inherit the 3D extension of Fuchs et al. (2020) based on the N-body simulation introduced in Kipf et al. (2018). For each trajectory, we provide the initial states of the system $\{\boldsymbol{S}_i^0\}_{i=1}^N$, the particles' charges $\{c_i \in (-1, 1)\}_{i=1}^N$ and a configuration indicating which particles are connected by sticks or hinges. Similar to Satorras et al. (2021), the task is to predict the final positions $\{\boldsymbol{x}_i^T\}_{i=1}^N$ of the particles when $T = 1000$. The validation and testing sets contain 2000 trajectories. We evaluate the prediction error by the MSE metric. Compared with the simulation conducted in Fuchs et al. (2020); Satorras et al. (2021), our dataset is more challenging in three senses: **1.** We consider systems with multiple scales, including 5, 10, and 20 particles in total, respectively. **2.** We introduce to the system the dynamics of hinges and sticks (depicted in Appendix § B), and construct various combinations between these objects. **3.** We investigate the performance of each model across different scales of training set, *e.g.*, 500 and 1500, to see how the models perform with scarce or relatively abundant training data.

Implementation details. Following Satorras et al. (2021), we use a linear mapping of the scale of initial velocity $||\boldsymbol{v}_i^0||_2$ as the input node feature h_i^0. The edge feature is provided by a concatenation of the product of charges $\boldsymbol{c}_i\boldsymbol{c}_j$ and an edge type indicator I_{ij}, where I_{ij} is valued as 0 if node i and j are disconnected, 1 if connected by a stick, and 2 if connected by a hinge. Note that this edge type indicator is an augmentation over the original setting in EGNN, designed to enforce EGNN and other baselines the ability to distinguish different types of edges, namely, with or without constraints. Other settings including the hyper-parameters are introduced in Appendix § D.

4.1 RESULTS

Comparison with SOTAs. Table 1 reports the performance of GMN and various compared models: EGNN (Satorras et al., 2021) and its regulated version EGNNReg, SE3-Transformer (Fuchs et al., 2020), Radial-Field (RF) (Köhler et al., 2019), Tensor-Field-Network (TFN) (Thomas et al., 2018), and other two baselines, GNN and the Linear prediction (Satorras et al., 2021). Regarding EGNN and EGNNReg, they share the same backbones (*i.e.* φ_1 and ψ) and training hyper-parameters (learning rates, layer number, etc) with our GMN for a fair comparison. For EGNNReg, we explicitly involve a regularization term during training by enforcing the geometrical constraints, namely preserving the lengths between two particles on sticks and hinges; the regularization factor is ranged from 0.01 to 0.1, where the value giving the best performance is selected. The default settings of SE3-Transformer and TFN perform poorly on our experiments, hence we have tried our best to tune their hyper-parameters by validation. In Table 1, the experiments are conducted on various types of systems consisting of p isolated particles, s sticks and h hinges, abbreviated as (p, s, h). We evaluate two distinct cases by using 500 and 1500 training systems, respectively.

From Table 1, we have these observations: **1.** GMN clearly outperforms all compared methods on all scenarios, suggesting the consistent superiority of our proposed methodology on constrained systems. **2.** GMN is more robust when the complexity of the system increases. On $|\text{Train}| = 500$, for example, the performance of GMN degenerates slightly by increasing the number of sticks (*e.g.* from

Table 2: Constraint error on various types of systems.

	|Train| = 500					|Train| = 1500				
	1,2,0	2,0,1	3,2,1	0,10,0	5,3,3	1,2,0	2,0,1	3,2,1	0,10,0	5,3,3
GNN	0.200	0.386	0.492	0.154	0.468	0.225	0.426	0.779	0.251	0.772
EGNN	0.220	0.370	0.714	0.248	0.760	0.217	0.317	0.521	0.139	0.596
EGNNReg	0.172	0.146	0.232	0.198	0.241	0.159	0.053	0.091	0.097	0.075
GMN	**0.000**	**0.000**	**0.000**	**0.000**	**0.000**	**0.000**	**0.000**	**0.000**	**0.000**	**0.000**

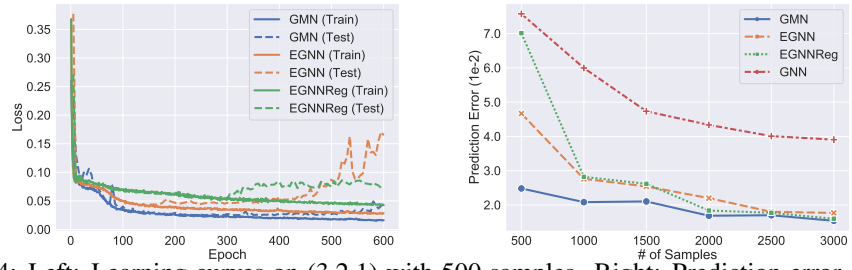

Figure 4: Left: Learning curves on (3,2,1) with 500 samples. Right: Prediction error on different training sizes on (3,2,1).

(1,2,0) to (0,10,0)), or increasing the number of particles and hinges (*e.g.* from (1,2,0) to (3,2,1)), while other methods (such as EGNN) drops significantly in both cases. **3.** Reducing the training size will hinder the performance of all compared methods remarkably. On the contrary, GMN still performs promisingly in general. For instance, on (3,2,1), EGNNReg becomes much worse from 2.62 to 7.01 when the volume of training data is decreased from 1500 to 500, whereas the change of GMN is smaller (2.10 v.s. 2.48). This is reasonable as GMN meets constraints spontaneously as opposed to EGNN and EGNNReg that learn to remember constraints by training.

Fig. 4 (Left) displays the learning curves for GMN, EGNN and EGNNReg. It shows GMN converges faster, and behaves better in preventing over-fitting against other methods.

Constraint satisfaction. One vital feature of GMN is that it maintains the geometrical constraints exactly and inherently. To show this, Table 2 records the corresponding constraint errors of several typical models. The results do verify our claim that GMN always outputs near-zero errors (all below 1e-4). Although EGNNReg that augments EGNN with regulation helps in reducing the constraint errors, it is data-driven and limited by the number of training samples; further, the constraints are pursued softly, making it defective for the applications where hard constraints are indispensable.

How the size of the training set influences. Fig. 4 depicts the prediction errors when the training size varies. It is observed that GMN acts steadily, justifying its benefit in data efficiency. Once again, both EGNN and EGNNReg deliver much worse performance when the training size is small, and they approach GMN when the training dataset is enlarged sufficiently. In physics, it is important to ensure the physics rules that are discovered by a relatively small number of experiments to be general enough for explaining universal phenomena. Hence, data efficiency, as a key advantage of GMN, comes as an important requirement for learning to model physical systems. Besides, by the comparison between GNN and other equivariant models, it is seen that equivariance is a crucial point for performance guarantee.

The generalization capability across different systems. In addition to the generalization in terms of training size, it is interesting to check how the models perform when trained on one system but tested on others. For this goal, Table 3 tests the generalization from (3,2,1) to (2,4,0) and (1,0,3). Interestingly, the performances of all models on new systems are comparable with the original environment (3,2,1). We conjecture that this ability could be attributed to the usage of GNN in capturing the combination diversity of the objects. As before, GMN achieves the least errors on all cases.

Ablation studies: 1. The function φ_2 is designed to be equivariant in Eq. 12. To justify this necessity, we replace φ_2 with an MLP of the same size, and report the errors in Table 4, from which we confirm that removing equivariance incurs detriment to the performance. **2.** The default setting of GMN in Eq. 6 is leveraging unshared acceleration inference $\varphi_2(\boldsymbol{f}_i^l)$ for sticks and

Table 3: Generalization across different systems. All models are trained on the (3,2,1) scenario.

	|Train| = 500				|Train| = 1500			
	3,2,1	2,4,0	1,0,3	Average	3,2,1	2,4,0	1,0,3	Average
GNN	7.58	8.06	8.37	8.00	4.73	4.98	5.58	5.10
EGNN	4.67	3.42	4.40	4.16	2.54	2.75	3.49	2.93
EGNNReg	7.01	4.49	6.62	6.04	2.62	2.62	4.29	3.18
GMN	**2.48**	**2.53**	**3.28**	**2.76**	**2.10**	**2.18**	**2.65**	**2.31**

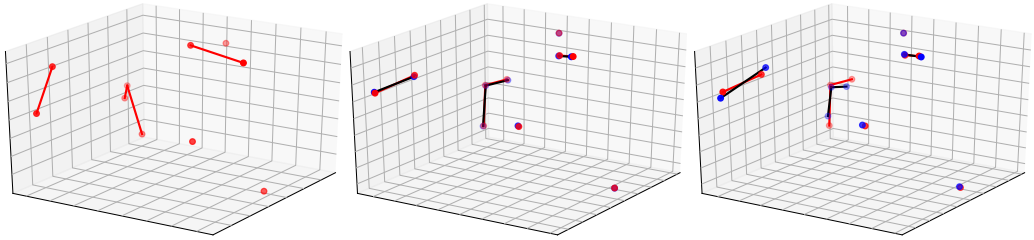

Figure 5: Left: initial position. Middle: the prediction of GMN (in blue). Right: the prediction of EGNN (in blue). Ground truth is marked in red. Better viewed by zooming in.

$\varphi_2(\boldsymbol{f}_i^l, \boldsymbol{x}_{ki}^{l-1}, \boldsymbol{v}_{ki}^{l-1})$ for hinges. Here we investigate different cases by assigning the identical form of φ_2 for sticks and hinges with shared or unshared parameters. Applying identical $\varphi_2(\boldsymbol{f}_i^l, \boldsymbol{x}_{ki}^{l-1}, \boldsymbol{v}_{ki}^{l-1})$ mostly outperforms the case by using $\varphi_2(\boldsymbol{f}_i^l)$, probably owing to the better expressivity of the former version. Yet, both cases are worse than our design, implying that the dynamics of sticks and hinges should be modeled distinctly. **3.** We have introduced an normalization term in Eq. 12. Table 4 demonstrates that eliminating this term leads to divergence during training, possibly owing to he numerical instability in the forward/backward propagation.

Table 4: Ablation Studies on GMN. "O.F." denotes numerical over-flow.

	|Train| = 500		|Train| = 1500	
	3,2,1	5,3,3	3,2,1	5,3,3
GMN	**2.48**	**4.08**	**2.10**	**2.86**
w/o Equivariance	3.74	4.41	2.46	3.29
φ_2 with $(\boldsymbol{f}_i^l, \boldsymbol{x}_{ki}^{l-1}, \boldsymbol{v}_{ki}^{l-1})$	2.86	4.15	2.20	3.00
φ_2 with $(\boldsymbol{f}_i^l, \boldsymbol{x}_{ki}^{l-1}, \boldsymbol{v}_{ki}^{l-1})$, shared	3.86	4.25	2.30	3.10
φ_2 with only $\boldsymbol{f}_i^l$	3.10	4.39	2.34	4.19
φ_2 with only $\boldsymbol{f}_i^l$, shared	2.91	4.94	2.39	3.45
w/o Normalization	3.15	O.F.	O.F.	O.F.

Visualization. We have also visualized the prediction outcomes by GMN and EGNN in Fig. 5. GMN is found to be able to track the ground-truth trajectories accurately, whereas EGNN yields clear position errors and particularly breaks the constraints for sticks and hinges. These results are consistent with the performance in Table 1.

5 Conclusion

In this paper, we propose Graph Mechanics Networks (GMN) that are capable of characterising constrained systems of interacting objects. The core of GMN is making use of generalized coordinates, by which the constraints are implicitly and exactly encapsulated in the forward kinematics. To enable Euclidean symmetry, we have developed a general form of equivariant functions to simulate the interaction forces and backward dynamics, whose expressivity is theoretically justified. We leverage sticks, hinges, and the combination of them with isolated particles as empirical examples that have verified the advantages of GMN over existing methods regarding prediction error, constraint satisfaction and data efficiency. As an initial attempt, we hope our work can facilitate more studies of learning to model more practical interacting systems in the future.

6 REPRODUCIBILITY STATEMENT

The complete proof of the theorems is provided in Appendix § A. The hyper-parameters and other experimental details are provided in Appendix § D.

Our code is available at: https://github.com/GraphMechanicsNetwork/GraphMechanicsNetwork.

7 ETHICS STATEMENT

The research in this paper does NOT involve any human subject, and our dataset is not related to any issue of privacy and can be used publicly. All authors of this paper follow the ICLR Code of Ethics (https://iclr.cc/public/CodeOfEthics).

REFERENCES

Peter W Battaglia, Razvan Pascanu, Matthew Lai, Danilo Rezende, and Koray Kavukcuoglu. Interaction networks for learning about objects, relations and physics. *arXiv preprint arXiv:1612.00222*, 2016.

George Cybenko. Approximation by superpositions of a sigmoidal function. *Mathematics of control, signals and systems*, 2(4):303–314, 1989.

Marc Finzi, Samuel Stanton, Pavel Izmailov, and Andrew Gordon Wilson. Generalizing convolutional neural networks for equivariance to lie groups on arbitrary continuous data. In *International Conference on Machine Learning*, pp. 3165–3176. PMLR, 2020a.

Marc Finzi, Ke Alexander Wang, and Andrew Gordon Wilson. Simplifying hamiltonian and lagrangian neural networks via explicit constraints. *arXiv preprint arXiv:2010.13581*, 2020b.

Fabian B Fuchs, Daniel E Worrall, Volker Fischer, and Max Welling. Se (3)-transformers: 3d roto-translation equivariant attention networks. *arXiv preprint arXiv:2006.10503*, 2020.

Kurt Hornik. Approximation capabilities of multilayer feedforward networks. *Neural networks*, 4 (2):251–257, 1991.

Michael J Hutchinson, Charline Le Lan, Sheheryar Zaidi, Emilien Dupont, Yee Whye Teh, and Hyunjik Kim. Lietransformer: equivariant self-attention for lie groups. In *International Conference on Machine Learning*, pp. 4533–4543. PMLR, 2021.

Thomas Kipf, Ethan Fetaya, Kuan-Chieh Wang, Max Welling, and Richard Zemel. Neural relational inference for interacting systems. *arXiv preprint arXiv:1802.04687*, 2018.

Jonas Köhler, Leon Klein, and Frank Noé. Equivariant flows: sampling configurations for multi-body systems with symmetric energies. *arXiv preprint arXiv:1910.00753*, 2019.

Karolis Martinkus, Aurelien Lucchi, and Nathanaël Perraudin. Scalable graph networks for particle simulations. *AAAI*, 2021.

RV Mises and Hilda Pollaczek-Geiringer. Praktische verfahren der gleichungsauflösung. *ZAMM-Journal of Applied Mathematics and Mechanics/Zeitschrift für Angewandte Mathematik und Mechanik*, 9(1):58–77, 1929.

Damian Mrowca, Chengxu Zhuang, Elias Wang, Nick Haber, Li Fei-Fei, Joshua B Tenenbaum, and Daniel LK Yamins. Flexible neural representation for physics prediction. *arXiv preprint arXiv:1806.08047*, 2018.

Alvaro Sanchez-Gonzalez, Victor Bapst, Kyle Cranmer, and Peter Battaglia. Hamiltonian graph networks with ode integrators. *arXiv preprint arXiv:1909.12790*, 2019.

Victor Garcia Satorras, Emiel Hoogeboom, and Max Welling. E(n) equivariant graph neural networks. *arXiv preprint arXiv:2102.09844*, 2021.

Joshua B Tenenbaum, Charles Kemp, Thomas L Griffiths, and Noah D Goodman. How to grow a mind: Statistics, structure, and abstraction. *science*, 331(6022):1279–1285, 2011.

Nathaniel Thomas, Tess Smidt, Steven Kearnes, Lusann Yang, Li Li, Kai Kohlhoff, and Patrick Riley. Tensor field networks: Rotation-and translation-equivariant neural networks for 3d point clouds. *arXiv preprint arXiv:1802.08219*, 2018.

Zonghan Wu, Shirui Pan, Fengwen Chen, Guodong Long, Chengqi Zhang, and S Yu Philip. A comprehensive survey on graph neural networks. *IEEE transactions on neural networks and learning systems*, 32(1):4–24, 2020.

Shuqi Yang, Xingzhe He, and Bo Zhu. Learning physical constraints with neural projections. *arXiv preprint arXiv:2006.12745*, 2020.

A THE PROOF OF THEOREM 1

In the following, we define the orthogonal group as $\mathcal{O}(d) = \{\boldsymbol{O} \in \mathbb{R}^{d\times d} \mid \boldsymbol{O}^\top\boldsymbol{O} = \boldsymbol{O}\boldsymbol{O}^\top = \boldsymbol{I}_d\}$ Prior to providing the proof for Theorem 1, we first list two necessary lemmas below.

Lemma 1. *For any two matrices $\boldsymbol{Z}_1, \boldsymbol{Z}_2 \in \mathbb{R}^{d\times m}$, we have this equivalence: $\exists \boldsymbol{O} \in \mathcal{O}(d), \boldsymbol{O}\boldsymbol{Z}_1 = \boldsymbol{Z}_2 \Leftrightarrow \boldsymbol{Z}_1^\top\boldsymbol{Z}_1 = \boldsymbol{Z}_2^\top\boldsymbol{Z}_2$.*

Proof. We only need to prove the "$\Leftarrow$" direction, as "$\Rightarrow$" holds clearly. Suppose the SVD decomposition of $\boldsymbol{Z}_1$ as $\boldsymbol{Z}_1 = \boldsymbol{U}_1\boldsymbol{S}_1\boldsymbol{V}_1^\top$ with the left-singular matrix $\boldsymbol{U}_1 \in \mathcal{O}(d)$, the singular diagonal matrix $\boldsymbol{S}_1 \in \mathbb{R}^{d\times m}$, and the right-singular matrix $\boldsymbol{V}_1 \in \mathcal{O}(m)$. Since $\boldsymbol{Z}_1^\top\boldsymbol{Z}_1 = \boldsymbol{Z}_2^\top\boldsymbol{Z}_2$, then there must exists a certain SVD decomposition of $\boldsymbol{Z}_2$ that shares the same singular matrix and right-singular matrix with $\boldsymbol{Z}_1$, implying that $\boldsymbol{Z}_2 = \boldsymbol{U}_2\boldsymbol{S}_1\boldsymbol{V}_1^\top$, where $\boldsymbol{U}_2 \in \mathcal{O}(d)$. Hence, $\boldsymbol{Z}_2 = \boldsymbol{U}_2\boldsymbol{S}_1\boldsymbol{V}_1^\top = \boldsymbol{U}_2\boldsymbol{U}_1^\top\boldsymbol{U}_1\boldsymbol{S}_1\boldsymbol{V}_1^\top = \boldsymbol{U}_2\boldsymbol{U}_1^\top\boldsymbol{Z}_1$, which concludes the proof owing to the orthogonality of $\boldsymbol{U}_2\boldsymbol{U}_1^\top$. □

Lemma 2. *The function $f : \mathbb{R}^{d\times m} \to \mathbb{R}^{m'}$ is invariant on $\mathcal{O}(d)$, namely, $f(\boldsymbol{O}\boldsymbol{Z}) = f(\boldsymbol{Z}), \forall \boldsymbol{O} \in \mathcal{O}(d), \forall \boldsymbol{Z} \in \mathbb{R}^{d\times m}$, if and only if there exists function $g : \mathbb{R}^{m\times m} \to \mathbb{R}^{m'}$ satisfying $f(\boldsymbol{Z}) = g(\boldsymbol{Z}^\top\boldsymbol{Z})$.*

Proof. The sufficiency is obvious. We now prove the necessity. We define the equivalence class $[\boldsymbol{Z}_0] = \{\boldsymbol{Z} \mid \exists \boldsymbol{O} \in \mathcal{O}(d), \boldsymbol{O}\boldsymbol{Z} = \boldsymbol{Z}_0\}$. Since f is invariant to the orthogonal transformation, it means f is actually a function on the equivalence class, *i.e.*, $f(\boldsymbol{Z}) = f([\boldsymbol{Z}])$. On the other hand, according to Lemma 1, we have $[\boldsymbol{Z}_1] = [\boldsymbol{Z}_2] \Leftrightarrow \boldsymbol{Z}_1^\top\boldsymbol{Z}_1 = \boldsymbol{Z}_2^\top\boldsymbol{Z}_2$, which implies the one-to-one correspondence between $[\boldsymbol{Z}]$ and $\boldsymbol{Z}^\top\boldsymbol{Z}$; hence, there must exist a function f' leading to $[\boldsymbol{Z}] = f'(\boldsymbol{Z}^\top\boldsymbol{Z})$, and f' is continuous in terms of any invariant metric such as the norm $\|\boldsymbol{Z}^\top\boldsymbol{Z}\|$. Overall, $f(\boldsymbol{Z}) = f([\boldsymbol{Z}]) = f(f'(\boldsymbol{Z}^\top\boldsymbol{Z})) \coloneqq g(\boldsymbol{Z}^\top\boldsymbol{Z})$. □

We are now ready to prove Theorem 1 that is copied below for better readability.

Theorem 1. *If $m \geq d$ and the row rank of $\boldsymbol{Z}$ is full,* i.e. *rank$(\boldsymbol{Z}) = d$, then for any continuous orthogonality-equivariant function $\hat{\varphi}(\boldsymbol{Z}, h)$, there must exist an MLP ρ_w satisfying $\|\varphi(\boldsymbol{Z}, h) - \hat{\varphi}(\boldsymbol{Z}, h)\| < \epsilon$ for arbitrarily small error ϵ.*

Proof. Without loss of generality, we will omit the non-vector term h, which does not change the story but let our proof more concise. Because $\boldsymbol{Z}$ is of full row-rank, the columns of an arbitrary function $\hat{\varphi}(\boldsymbol{Z})$ can be represented as a linear combination of the columns of $\boldsymbol{Z}$; in other words, there must exist a function $\pi : \mathbb{R}^{d\times m} \to \mathbb{R}^{m\times m'}$ giving rise to $\hat{\varphi}(\boldsymbol{Z}) = \boldsymbol{Z}\pi(\boldsymbol{Z})$. Considering the orthogonality-equivariance, we derive the property of $\pi(\boldsymbol{Z})$ as:

$$\begin{aligned} \hat{\varphi}(\boldsymbol{O}\boldsymbol{Z}) &= \boldsymbol{O}\hat{\varphi}(\boldsymbol{Z}), \\ \Rightarrow \boldsymbol{O}\boldsymbol{Z}\pi(\boldsymbol{O}\boldsymbol{Z}) &= \boldsymbol{O}\boldsymbol{Z}\pi(\boldsymbol{Z}), \\ \Rightarrow \boldsymbol{Z}\pi(\boldsymbol{O}\boldsymbol{Z}) &= \boldsymbol{Z}\pi(\boldsymbol{Z}). \end{aligned} \tag{15}$$

Since $d \leq m$ and the row-rank of $\boldsymbol{Z}$ is full, we perform the compact SVD decomposition on $\boldsymbol{Z}$, namely, $\boldsymbol{Z} = \boldsymbol{U_Z}\boldsymbol{S_Z}\boldsymbol{V_Z}^\top$, where $\boldsymbol{U_Z} \in \mathcal{O}(d)$, $\mathbb{R}^{d\times d} \ni \boldsymbol{S_Z} > 0$, and $\boldsymbol{V_Z} \in \mathbb{R}^{m\times d}$ satisfying $\boldsymbol{V_Z}^\top\boldsymbol{V_Z} = \boldsymbol{I}_d$. Eq. 15 becomes:

$$\begin{aligned} \boldsymbol{Z}\pi(\boldsymbol{O}\boldsymbol{Z}) &= \boldsymbol{Z}\pi(\boldsymbol{Z}), \\ \Rightarrow \boldsymbol{U_Z}\boldsymbol{S_Z}\boldsymbol{V_Z}^\top\pi(\boldsymbol{O}\boldsymbol{Z}) &= \boldsymbol{U_Z}\boldsymbol{S_Z}\boldsymbol{V_Z}^\top\pi(\boldsymbol{Z}), \\ \Rightarrow \boldsymbol{S_Z}\boldsymbol{V_Z}^\top\pi(\boldsymbol{O}\boldsymbol{Z}) &= \boldsymbol{S_Z}\boldsymbol{V_Z}^\top\pi(\boldsymbol{Z}). \end{aligned} \tag{16}$$

Given that $\boldsymbol{S_Z} = \text{Eigen}(\boldsymbol{Z}^\top\boldsymbol{Z})$ and $\boldsymbol{V_Z} = \text{EigenVector}(\boldsymbol{Z}^\top\boldsymbol{Z})$ are respectively the eigenvalues and eigenvectors of $\boldsymbol{Z}^\top\boldsymbol{Z}$ and are clearly invariant to the orthogonal transformation of $\boldsymbol{Z}$. Their values can be numerically approximated by iterative programs, such as the power method (Mises & Pollaczek-Geiringer, 1929), thus can be treated as the continuous functions of $\boldsymbol{Z}^\top\boldsymbol{Z}$. Let us define $g'(\boldsymbol{Z}) \coloneqq \boldsymbol{S_Z}\boldsymbol{V_Z}^\top\pi(\boldsymbol{Z})$. Then, we keep deriving Eq. 16 by:

$$\begin{aligned} \boldsymbol{S_Z}\boldsymbol{V_Z}^\top\pi(\boldsymbol{O}\boldsymbol{Z}) &= \boldsymbol{S_Z}\boldsymbol{V_Z}^\top\pi(\boldsymbol{Z}), \\ \Rightarrow \boldsymbol{S_{OZ}}\boldsymbol{V_{OZ}}^\top\pi(\boldsymbol{O}\boldsymbol{Z}) &= \boldsymbol{S_Z}\boldsymbol{V_Z}^\top\pi(\boldsymbol{Z}), \\ \Rightarrow g'(\boldsymbol{O}\boldsymbol{Z}) &= g'(\boldsymbol{Z}). \end{aligned} \tag{17}$$

According to Lemma 2, the function g satisfies Eq. 17 if and only if it is written as $g'(\boldsymbol{Z}) = g(\boldsymbol{Z}^\top\boldsymbol{Z})$ for a certain function g. By checking the formulation of $\hat{\varphi}(\boldsymbol{Z})$ as demonstrated before, we arrive at

$$\begin{aligned} \hat{\varphi}(\boldsymbol{Z}) &= \boldsymbol{Z}\pi(\boldsymbol{Z}), \\ &= \boldsymbol{U_Z}\boldsymbol{S_Z}\boldsymbol{V_Z}^\top\pi(\boldsymbol{Z}), \\ &= \boldsymbol{U_Z}g'(\boldsymbol{Z}), \\ &= \boldsymbol{U_Z}g(\boldsymbol{Z}^\top\boldsymbol{Z}), \\ &= \boldsymbol{U_Z}\boldsymbol{S_Z}\boldsymbol{V_Z}^\top\boldsymbol{V_Z}\boldsymbol{S_Z}^{-1}g(\boldsymbol{Z}^\top\boldsymbol{Z}), \\ &= \boldsymbol{Z}\boldsymbol{V_Z}\boldsymbol{S_Z}^{-1}g(\boldsymbol{Z}^\top\boldsymbol{Z}), \\ &\coloneqq \boldsymbol{Z}\eta(\boldsymbol{Z}^\top\boldsymbol{Z}). \end{aligned} \tag{18}$$

Here the function η can be approximated by MLP whose universality has been justified by (Cybenko, 1989; Hornik, 1991). The conclusion of Theorem 1 is proved.

□

Corollary 1. *Assume $m \geq d$, and also the entries of $\boldsymbol{Z}$ are drawn independently from a distribution that is absolutely continuous with respect to the Lebesgue measure in $\mathbb{R}$. Then, almost surely, the conclusion of Theorem 1 holds.*

Proof. This is straightforward. When $\text{rank}(\boldsymbol{Z}) < d$, the columns of $\boldsymbol{Z}$ are located in a subspace of $\mathbb{R}^d$ (for example a line or a plane in the 3D space), whose measure is zero. Therefore, the probability for making $\text{rank}(\boldsymbol{Z}) = d$ is 1, and we almost surely have the same conclusion as Theorem 1. □

Corollary 2. *For any continuous orthogonality-equivariant function $\hat{\varphi}(\boldsymbol{Z}, h)$ whose output is located in the linear subspace expanded by the columns of $\boldsymbol{Z}$, the conclusion of Theorem 1 holds universally.*

Proof. According to the definition of $\hat{\varphi}(\boldsymbol{Z})$, we still obtain $\hat{\varphi}(\boldsymbol{Z}) = \boldsymbol{Z}\pi(\boldsymbol{Z})$. Let us assume $d > m$ (otherwise we can directly obtain Theorem 1), then the full SVD decomposition of $\boldsymbol{Z}$ is $\boldsymbol{Z} = \boldsymbol{U_Z}\boldsymbol{S_Z}\boldsymbol{V_Z}^\top$, with $\boldsymbol{U_Z} \in \mathcal{O}(d)$, $\boldsymbol{S_Z} \in \mathbb{R}^{d\times m}$, and $\boldsymbol{V_Z} \in \mathcal{O}(m)$. But here, $\boldsymbol{S_Z}$ is not strictly positive. Suppose $\boldsymbol{S_Z} = \begin{pmatrix} \boldsymbol{S}_+ \\ \boldsymbol{0} \end{pmatrix}$, where $\boldsymbol{S}_+ > 0$. We retain that $\boldsymbol{S_Z}\boldsymbol{V_Z}^\top\pi(\boldsymbol{Z}) = g(\boldsymbol{Z}^\top\boldsymbol{Z})$ by imitating the proof in Eq. 15-17. Analogous to Eq. 18, we derive,

$$\begin{aligned} \hat{\varphi}(\boldsymbol{Z}) &= \boldsymbol{Z}\pi(\boldsymbol{Z}), \\ &= \boldsymbol{U_Z}g(\boldsymbol{Z}^\top\boldsymbol{Z}), \\ &= \boldsymbol{U_Z}\boldsymbol{S_Z}\boldsymbol{V_Z}^\top\boldsymbol{V_Z}\left(\boldsymbol{S}_+^{-1}, \boldsymbol{0}\right)g(\boldsymbol{Z}^\top\boldsymbol{Z}), \\ &= \boldsymbol{Z}\boldsymbol{V_Z}\left(\boldsymbol{S}_+^{-1}, \boldsymbol{0}\right)g(\boldsymbol{Z}^\top\boldsymbol{Z}), \\ &\coloneqq \boldsymbol{Z}\eta(\boldsymbol{Z}^\top\boldsymbol{Z}), \end{aligned} \tag{19}$$

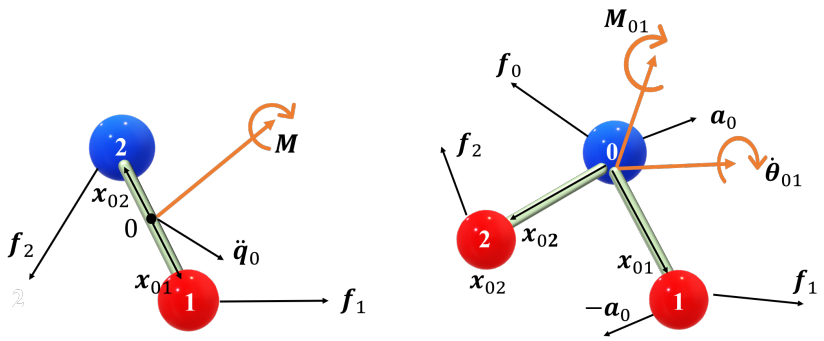

Figure 6: Left: Dynamics of sticks. Right: Dynamics of hinges.

which concludes the proof.

□

B THE DYNAMICS ANALYSES FOR STICKS AND HINGES

The analytical forms of the dynamics for sticks and hinges can be found from a mechanics book. Here we derive the formulas on our own to make our paper more self-contained. For simplicity, we consider all particles to be of the equal mass and the sticks of no mass.

Dynamics analysis of sticks. In Fig. 6 (Left), we assume the forces acting on particles 1 and 2 are separately $\boldsymbol{f}_1$ and $\boldsymbol{f}_2$. By following the theorem of the motion of the center of mass, the acceleration of the center is given by

$$\ddot{\boldsymbol{q}}_0 = \frac{\boldsymbol{f}_1 + \boldsymbol{f}_2}{m}. \tag{20}$$

The rotation accelerations of particles 1 and 2 around the center are calculated by

$$\ddot{\boldsymbol{\theta}}_{01} = \ddot{\boldsymbol{\theta}}_{02} = \frac{\boldsymbol{M}}{J} = \frac{\boldsymbol{x}_{01} \times \boldsymbol{f}_1 + \boldsymbol{x}_{02} \times \boldsymbol{f}_2}{m\|\boldsymbol{x}_{01}\|^2 + m\|\boldsymbol{x}_{02}\|^2}, \tag{21}$$

where $\boldsymbol{M}$ defines the total torque and J is the moments of inertia.

Dynamics analysis of hinges. The analysis for hinges is more complicated than sticks. In Fig. 6 (Right), the forces on particles 0, 1 and 2 are $\boldsymbol{f}_0$, $\boldsymbol{f}_1$ and $\boldsymbol{f}_2$. By using Newton's second law,

$$\boldsymbol{a}_0 + \boldsymbol{a}_1 + \boldsymbol{a}_2 = \frac{\boldsymbol{f}}{m}, \tag{22}$$

where the aggregated force is $\boldsymbol{f} = \boldsymbol{f}_0 + \boldsymbol{f}_1 + \boldsymbol{f}_2$. In addition, the kinematics relations between the three particles show that

$$\boldsymbol{a}_1 = \boldsymbol{a}_0 + \ddot{\boldsymbol{\theta}}_{01} \times \boldsymbol{x}_{01} + \dot{\boldsymbol{\theta}}_{01} \times \boldsymbol{\nu}_{\mathbf{01}}, \tag{23}$$

$$\boldsymbol{a}_2 = \boldsymbol{a}_0 + \ddot{\boldsymbol{\theta}}_{02} \times \boldsymbol{x}_{02} + \dot{\boldsymbol{\theta}}_{02} \times \boldsymbol{\nu}_{\mathbf{02}}, \tag{24}$$

where $\dot{\boldsymbol{\theta}}_{01}$ and $\ddot{\boldsymbol{\theta}}_{01}$ denote the speed and acceleration of the rotation angle of particle 1 around 0, and $\boldsymbol{\nu}_{\mathbf{01}}$ is the corresponding linear velocity; the symbols $\dot{\boldsymbol{\theta}}_{02}$, $\ddot{\boldsymbol{\theta}}_{02}$ and $\boldsymbol{\nu}_{\mathbf{02}}$ are defined similarly. Moreover, the relative rotation acceleration of particle 1 to 0 is caused by the external force $\boldsymbol{f}_1$ and the inertia force $-m\boldsymbol{a}_0$ acting on 1, which derives that

$$\ddot{\boldsymbol{\theta}}_{01} = \frac{\boldsymbol{M}_{01}}{J_{01}} = \frac{\boldsymbol{x}_{01} \times (\boldsymbol{f}_1 - m\boldsymbol{a}_0)}{m\|\boldsymbol{x}_{01}\|^2}. \tag{25}$$

Analogously,

$$\ddot{\boldsymbol{\theta}}_{02} = \frac{\boldsymbol{M}_{02}}{J_{02}} = \frac{\boldsymbol{x}_{02} \times (\boldsymbol{f}_2 - m\boldsymbol{a}_0)}{m\|\boldsymbol{x}_{02}\|^2}. \tag{26}$$

After substituting Eq. 25 into Eq. 23, and Eq. 26 into Eq. 24, and then rearranging Eq. 22, we have

$$\boldsymbol{a}_0 = (\boldsymbol{I} + \boldsymbol{e}_{01}\boldsymbol{e}_{01}^\top + \boldsymbol{e}_{02}\boldsymbol{e}_{02}^\top)^{-1}\boldsymbol{a}, \tag{27}$$

where $\boldsymbol{a} = \frac{\boldsymbol{f}}{m} - \dot{\boldsymbol{\theta}}_{01} \times \boldsymbol{\nu_{01}} - \dot{\boldsymbol{\theta}}_{02} \times \boldsymbol{\nu_{02}} - (\boldsymbol{I} - \boldsymbol{e}_{01}\boldsymbol{e}_{01}^\top)\frac{\boldsymbol{f}_1}{m} - (\boldsymbol{I} - \boldsymbol{e}_{02}\boldsymbol{e}_{02}^\top)\frac{\boldsymbol{f}_2}{m}$ with $\boldsymbol{e}_{01}$ and $\boldsymbol{e}_{02}$ represent the unit vectors along $\boldsymbol{x}_{01}$ and $\boldsymbol{x}_{02}$, respectively. We have applied a trick to simplify the derivation by observing $\frac{\boldsymbol{x}_{01} \times \boldsymbol{f}_1 \times \boldsymbol{x}_{01}}{\|\boldsymbol{x}_{01}\|^2} = (\boldsymbol{I} - \boldsymbol{e}_{01}\boldsymbol{e}_{01}^\top)\boldsymbol{f}_1$. Besides, $\boldsymbol{I} + \boldsymbol{e}_{01}\boldsymbol{e}_{01}^\top + \boldsymbol{e}_{02}\boldsymbol{e}_{02}^\top$ is invertible, hence Eq. 27 is always meaningful.

Substituting Eq. 27 back into Eq. 25 and Eq. 26 derives the values of $\ddot{\boldsymbol{\theta}}_{01}$ and $\ddot{\boldsymbol{\theta}}_{02}$. Note that in § 3.4, we employ the denotation of generalized coordinates by $\boldsymbol{q}_0$, $\dot{\boldsymbol{q}}_0$ and $\ddot{\boldsymbol{q}}_0$ which indeed share the same meaning with the Cartesian coordinates $\boldsymbol{x}_0$, $\boldsymbol{v}_0$ and $\boldsymbol{a}_0$ of particle 0.

C FULL ALGORITHMIC DETAILS

In the main body of the paper, for better readability, we first introduce the general pipeline of our method in § 3.2 and then present the implementation details by taking the angels into account in § 3.4. Here, we combine them into one singe algorithmic flowchart in Alg. 1.

D MORE EXPERIMENTAL DETAILS AND RESULTS

Hyper-parameters. For GNN, RF, EGNN, EGNNReg, and GMN, we empirically find that the following hyper-parameters generally work well, and use them across all experimental evaluations: batch size 200, learning rate 0.0005, hidden dim 64, and weight decay 1×10^{-10}. SE3-Transformer and TFN do not perform well on our datasets, potentially due to the challenge of highly complex systems. Consequently, we tune the hyper-parameters and adopt the following configuration: batch size 100, learning rate 0.001, hidden dim 64, representation degrees 3 and weight decay 1×10^{-8}. All models are evaluated with four layers, and are trained for 600 epochs.

Constraint error. The constraint error is computed as the total change in the lengths of sticks and hinges between the input and output, averaged per trajectory. Specifically, for hinges, the two edges are both considered. EGNNReg is a variant of EGNN that explicitly adds the constraint error into its training loss by a regularization factor of λ. In our experiments, we also treat λ as a hyper-parameter, and choose λ that yields the best performance within the range [0.01, 0.1].

More visualization results. We provide more visualization results in Fig. 7. It is clear to observe that our GMN produces much more accurate prediction than EGNN, while EGNN tends to stretch or squeeze the sticks and hinges, breaking the geometric constraints of rigid bodies.

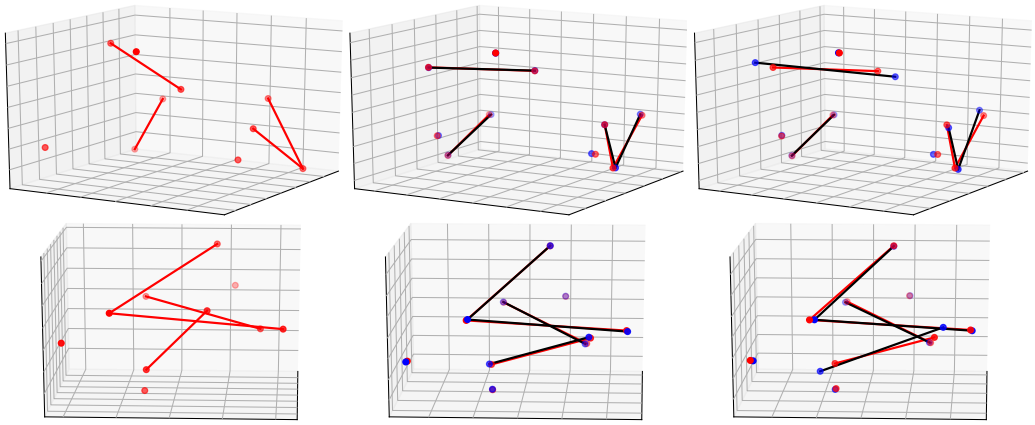

Figure 7: Left: initial position(s). Middle: the prediction(s) of GMN (in blue). Right: the prediction(s) of EGNN (in blue). Ground truth is marked in red. Better viewed by zooming in.

Algorithm 1 Graph Mechanics Networks (GMNs)

Input: Initial states of all particles $\{\boldsymbol{S}_i^0 = (\boldsymbol{x}_i^0, \boldsymbol{v}_i^0)\}_{i=1}^N$ and features $\{h_i^0\}_i^N$; Learnable equivariant functions $\varphi_1, \varphi_2, \psi, \psi'$; Layer number L.

Compute the generalized coordinates of all structural objects $\{(\boldsymbol{q}_k^0, \dot{\boldsymbol{q}}_k^0, \{\dot{\boldsymbol{\theta}}_{ki}^0\}_{i\in\mathcal{O}_k})\}_{k=1}^K$.

for layer $l = 1$ to L **do**

  for particle $i = 1$ to N **do**

    Calculate the interaction force $\boldsymbol{f}_i^l$ and feature h_i^l for each particle by:

$$\boldsymbol{f}_i^l, h_i^l = \sum_{j=1}^{N} \varphi_1(\boldsymbol{x}_{ji}^{l-1}, h_i^{l-1}, h_j^{l-1}, e_{ji}). \tag{28}$$

  end for

  for object $k = 1$ to K **do**

    Inference the generalized Cartesian acceleration $\ddot{\boldsymbol{q}}_k^l$ via:

$$\ddot{\boldsymbol{q}}_k^l = \sum_{i\in\mathcal{O}_k} \varphi_2(\boldsymbol{f}_i^l), \quad \text{(for sticks)} \tag{29}$$

$$\ddot{\boldsymbol{q}}_k^l = \sum_{i\in\mathcal{O}_k} \varphi_2(\boldsymbol{f}_i^l, \boldsymbol{x}_{ki}^{l-1}, \boldsymbol{v}_{ki}^{l-1}). \quad \text{(for hinges)} \tag{30}$$

    Derive the generalized angle acceleration:

$$\ddot{\boldsymbol{\theta}}_{ki} = \frac{\sum_{i\in\mathcal{O}_k} \boldsymbol{x}_{ki} \times \boldsymbol{f}_i}{\sum_{i\in\mathcal{O}_k} \|\boldsymbol{x}_{ki}\|^2}, \forall i \in \mathcal{O}_k, \quad \text{(for sticks)} \tag{31}$$

$$\ddot{\boldsymbol{\theta}}_{ki} = \frac{\boldsymbol{x}_{ki} \times (\boldsymbol{f}_i - \ddot{\boldsymbol{q}}_k)}{\|\boldsymbol{x}_{ki}\|^2}, \forall i \in \mathcal{O}_k. \quad \text{(for hinges)} \tag{32}$$

    Update the positions and velocities as follows:

$$\dot{\boldsymbol{q}}_k^l = \psi(\sum_{i\in\mathcal{O}_k} h_i^{l-1})\dot{\boldsymbol{q}}_k^{l-1} + \ddot{\boldsymbol{q}}_k^l, \tag{33}$$

$$\boldsymbol{q}_k^l = \boldsymbol{q}_k^{l-1} + \dot{\boldsymbol{q}}_k^l, \tag{34}$$

$$\dot{\boldsymbol{\theta}}_{ki}^l = \psi'(\sum_{i\in\mathcal{O}_k} h_i^{l-1})\dot{\boldsymbol{\theta}}_{ki}^{l-1} + \ddot{\boldsymbol{\theta}}_{ki}^l, \forall i \in \mathcal{O}_k. \tag{35}$$

    Perform the forward kinematics for each particle in $\mathcal{O}_k$:

$$\boldsymbol{x}_i^l = \boldsymbol{q}_k^l + \mathrm{rot}(\dot{\boldsymbol{\theta}}_{ki}^l)\boldsymbol{x}_{ki}^{l-1}, \forall i \in \mathcal{O}_k, \tag{36}$$

$$\boldsymbol{v}_i^l = \dot{\boldsymbol{q}}_k^l + \dot{\boldsymbol{\theta}}_{ki}^l \times \boldsymbol{x}_{ki}^l, \forall i \in \mathcal{O}_k. \tag{37}$$

  end for

end for

Output: The predicted states of all particles $\{\boldsymbol{S}_i^L\}_{i=1}^N$.

More experimental results. In Table 5, we provide a comprehensive performance comparison of different models under more scenarios with 500 training samples. Clearly, GMN outperforms other models on all object combinations involved.

Table 5: Prediction error ($\times 10^{-2}$) on various types of systems. The first column "p, s, h" denotes the scenario with p isolated particles, s sticks and h hinges. Models are trained with 500 samples.

	GMN	EGNN	EGNNReg	GNN	TFN	SE3-Tr.	RF	Linear
1,2,0	1.84	2.81	2.94	5.33	11.54	5.54	3.50	8.23
2,0,1	2.02	2.27	2.66	5.01	9.87	5.14	3.07	7.55
2,4,0	2.34	3.59	3.87	8.05	11.30	9.22	5.37	10.10
0,5,0	2.54	4.13	4.29	8.63	11.92	9.83	5.94	10.48
7,0,1	2.39	2.66	3.41	7.05	10.67	8.38	4.66	9.71
1,0,3	3.21	4.56	5.14	8.32	11.62	9.57	5.91	9.90
3,2,1	2.48	4.67	7.01	7.58	11.66	8.95	5.25	9.76
4,8,0	3.69	4.79	7.09	9.65	12.05	11.21	7.59	11.45
0,10,0	2.92	4.75	5.03	9.83	13.43	11.42	7.59	11.36
8,0,4	3.37	4.17	5.32	9.49	11.72	11.12	7.51	11.44
2,0,6	4.06	5.06	5.58	10.13	12.13	11.74	8.15	11.61
5,3,3	4.08	4.59	6.31	9.77	12.23	11.59	7.73	11.62